The influence of porosity, crystallinity and interlayer adhesion on the tensile strength of 3D printed polylactic acid (PLA)

Natalia von Windheim
Duke University Pratt School of Engineering, Durham, North Carolina, USA
David W. Collinson
Northwestern University Robert R McCormick School of Engineering and Applied Science, Evanston, Illinois, USA
Trent Lau
Duke University Trinity College of Arts and Sciences, Durham, North Carolina, USA, and
L. Catherine Brinson and Ken Gall
Duke University Pratt School of Engineering, Durham, North Carolina, USA

Abstract

Purpose – The purpose of this study is to understand how printing parameters and subsequent annealing impacts porosity and crystallinity of 3D printed polylactic acid (PLA) and how these structural characteristics impact the printed material's tensile strength in various build directions.

Design/methodology/approach – Two experimental studies were used, and samples with a flat vs upright print orientation were compared. The first experiment investigates a scan of printing parameters and annealing times and temperatures above the cold crystallization temperature (T_{cc}) for PLA. The second experiment investigates annealing above and below T_{cc} at multiple points over 12 h.

Findings – Annealing above T_{cc} does not significantly impact the porosity but it does increase crystallinity. The increase in crystallinity does not contribute to an increase in strength, suggesting that co-crystallization across the weld does not occur. Atomic force microscopy (AFM) images show that weld interfaces between printed fibers are still visible after annealing above T_{cc}, confirming the lack of co-crystallization. Annealing below T_{cc} does not significantly impact porosity or crystallinity. However, there is an increase in tensile strength. AFM images show that annealing below T_{cc} reduces thermal stresses that form at the interfaces during printing and slightly "heals" the as-printed interface resulting in an increase in tensile strength.

Originality/value – While annealing has been explored in the literature, it is unclear how it affects porosity, crystallinity and thermal stresses in fused filament fabrication PLA and how those factors contribute to mechanical properties. This study explains how co-crystallization across weld interfaces is necessary for crystallinity to increase strength and uses AFM as a technique to observe morphology at the weld.

Keywords Fused deposition modeling, Tensile strength, Microstructure, Post-processing

Paper type Research paper

1. Introduction

Polylactic acid (PLA) has emerged as a popular filament for fused filament fabrication (FFF) 3D printing owing to its low melting temperature and reliable print morphologies. Owing to the layer-by-layer extrusion nature of FFF, printed parts have anisotropic mechanical behavior because of inherent weaknesses at the weld between fiber layers. This is true for all materials printed with FFF, including PLA. Tensile properties often closely match injection molded properties when printed fibers are oriented in the testing direction, but when printed fibers are oriented perpendicular to the testing direction there is a significant reduction in mechanical properties (Song *et al.*, 2017). FFF parts can be designed to accommodate anisotropy by orienting fibers in the direction most suitable for loading but many applications have complex loading profiles that will challenge weaknesses across the fiber to fiber weld present in subsequent layers.

It is well documented that printing parameters affect mechanical properties (Beniak *et al.*, 2018; Luzanin *et al.*, 2017; Rajpurohit and Dave, 2018, 2019; Yang *et al.*, 2019), but it is still unclear how the underlying structural factors that affect mechanical properties are influenced by printing parameters. This lack of understanding makes it difficult to select printing parameters to achieve optimal mechanical properties. Initial studies have shown that FFF processing conditions influence the coalescence of fibers (polymer

The current issue and full text archive of this journal is available on Emerald Insight at: **https://www.emerald.com/insight/1355-2546.htm**

Rapid Prototyping Journal
27/7 (2021) 1327–1336
 [ISSN 1355-2546]
[DOI 10.1108/RPJ-08-2020-0205]

AFOSR FA9550-14-1-0032-P00003, NSF BCS-1734981, Duke University Grant/Award Number: 291-0067. This work was also performed in part at the Duke University Shared Materials Instrumentation Facility (SMIF), a member of the North Carolina Research Triangle Nanotechnology Network (RTNN), which is supported by the National Science Foundation (award number ECCS-2025064) as part of the National Nanotechnology Coordinated Infrastructure (NNCI).

Received 25 August 2020
Revised 12 April 2021
Accepted 20 April 2021

chain diffusion across weld) (Seppala *et al.*, 2017), thermal stresses (D'Amico *et al.*, 2017; Li *et al.*, 2018), porosity (Tronvoll *et al.*, 2018), morphology and crystallinity (Mcilroy *et al.*, 2019). However, there is limited exploration of these factors' work in conjunction to dictate mechanical properties and how they can be leveraged to improve mechanical properties, either during printing or with thermal post-processing.

Annealing is a post-processing method that is hypothesized to improve the mechanical properties of FFF PLA, as it does for injection molded PLA (Carrasco *et al.*, 2010). One hypothesis is that annealing improves the properties of FFF PLA through increasing crystallinity at or across the weld (Mcilroy *et al.*, 2019). However, there is limited mechanical testing data in the literature that supports this hypothesis and it is unclear how annealing influences other factors including thermal stresses at the weld and porosity. Some studies have explored annealing of FFF PLA but have shown little improvement in mechanical properties, and most of them do not address the effect of fiber orientation and weld weakness (Song *et al.*, 2017; Torres *et al.*, 2015; Wang *et al.*, 2017; Liao *et al.*, 2019). When examining the impact of thermal annealing on changes in crystallinity and porosity, it is essential to consider loading modes with tensile stresses both parallel and perpendicular to the interfacial weld normal. Loading in tension perpendicular to the interfacial weld normal is a direct measure of weld strength while loading parallel to the weld normal assesses the materials' inherent strength in the essential absence of a weak weld region.

While it is typical for an increase in crystallinity to increase the basic strength of injection molded PLA, these studies fail to consider weld behavior innate to FFF PLA. In 3D printing "welding" literature, co-crystallization across an interface is necessary to increase strength (Northcutt *et al.*, 2018; Xue *et al.*, 2000). When crystallinity forms without co-crystallization, there is a weakening of properties (Xue *et al.*, 2000). Additionally, once crystallization begins during printing, fiber coalescence stops. Cold crystallization annealing can happen during printing with subsequent layer deposition (Srinivas *et al.*, 2018). So, while crystallinity may be increasing during the annealing of FFF PLA, there has not been an investigation into whether spherulites are co-crystallizing across the interface of FFF welds. The hypothesis that annealing will improve mechanical properties of FFF PLA does not account for weaknesses at the weld owing to crystallinity limiting polymer chain diffusion during printing and inhibiting co-crystallization during annealing.

The goal of this study is to understand how annealing impacts porosity, crystallinity and weld morphology to determine how those factors affect tensile strength depending on the orientation of printed fibers. This is done using two experimental approaches and comparing samples with a flat print orientation to samples with an upright print orientation. The first experiment investigates a scan of printing parameters and annealing times and temperatures above the cold crystallization temperature (T_{cc}) for PLA. The second experiment investigates annealing above and below T_{cc} at multiple points over 12 h.

2. Materials and methods

2.1 Polylactic acid fused filament fabrication processing

PLA (MatterHackers – PLA Pro filament) dogbones (ASTM D638 Type V, 1.5 mm thickness) for tensile testing were sliced using Ultimaker Cura and printed using an Ultimaker 3. PLA filament was placed in a drying oven for at least 6 h at 50°C before printing to remove moisture. While samples were printed to match ASTM D638 Type V geometry, some modification of testing standards are required owing to anisotropy of 3D printing processing (Aydin and Kucuk, 2018; Forster, 2015; Peker *et al.*, 2020). Based on previous research, dogbones were printed in best- and worst-case print orientation and raster pattern (Chacón *et al.*, 2017). Best-case dogbones were printed flat in the XY plane with fibers oriented parallel to testing direction [Figure 1(a)], and worst-case dogbones were printed upright in the YZ plane with fibers oriented perpendicular to testing direction [Figure 1(b)].

Layer height and print speed parameters were varied by selecting a low and high value – 0.1 and 0.3 mm for layer height, 20 and 60 mm/s for print speed (Table 1). All other print parameters were kept constant, some key parameters include a 205°C nozzle temperature, 60°C build plate and a 0.4 mm nozzle diameter.

2.2 Annealing of printed dogbones

After printing, dogbones were either tested as-printed or annealed before testing. Flat and YZ dogbones with print parameters A through D (Table 1) were annealed at 80 and 95°C for 15 min and 1 h. XY and YZ dogbones with print parameters B were additionally annealed at either 65°C (below T_{cc}) or 80°C (above T_{cc}) for 15 min, 1 h, 3 h, 6 h or 12 h. The glass transition temperature (T_g) of the PLA filament is 59.5°C, as measured with differential scanning calorimetry (DSC). A heating rate of 20°C/min and the second heat pass of a heat–cool–heat cycle was used to determine T_g. The anneal temperatures of 65 and 80°C were determined to be below/above T_{cc} through experimentally annealing samples and measuring crystallinity with DSC.

2.3 X-ray microcomputed tomography analysis

The porosity of printed dogbones was quantified using X-ray microcomputed tomography (MicroCT) (Nikon XTH 225 ST) and Avizo software. Dogbones were scanned with a voxel

Figure 1 Print orientation and tensile testing direction for XY (a) and YZ (b) samples

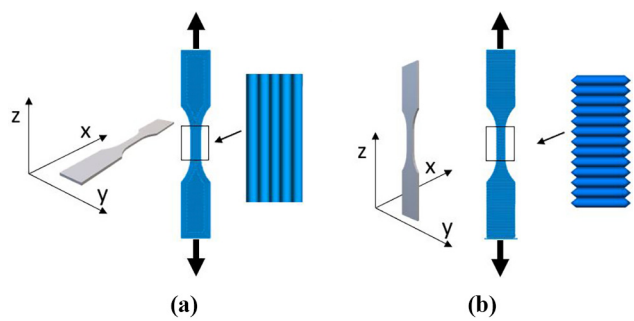

Table 1 A-D print parameters

Print parameters	Layer height	Print speed
A	0.1 mm	60 mm/s
B	0.1 mm	20 mm/s
C	0.3 mm	60 mm/s
D	0.3 mm	20 mm/s

size of 10.85 μm, 125 kV beam energy, 9.8 W and a 78 μA current. This resolution detects airgap porosity between printed fibers, but it is not fine enough to measure porosity within printed fibers. To analyze the airgap porosity, a subsection of the gauge section of each dogbone was selected. This subsection was thresholded to distinguish the solid and airgap fractions. The porosity reported is the airgap fraction of the total volume of the selected subsection.

2.4 Differential scanning calorimetry analysis

The crystallinity of the filament, as-printed and annealed, was determined using DSC (TA Discovery 2500). Approximately 10 mg was cut from dogbone samples and heated at 10°C/min in a nitrogen environment. The percent crystallinity was determined from the first pass ΔH_m divided by the theoretical ΔH_m of 93.64 J/g for 100% crystalline PLA (Fischer *et al.*, 1973).

2.5 Monotonic tensile testing

The stress–strain behavior of the printed dogbones was determined through monotonic tensile testing (Test Resources 830EL63) in accordance with ASTM D638 testing procedure. Dogbones were tested at a displacement rate of 1 mm/min until failure. Failure is defined as the fracture of one or all of the printed fibers in the sample resulting in a decrease in stress. The cross-section dimensions of samples were measured with calipers before testing. Strain was measured by marking tracking points on the sample before testing and using a video extensometer system.

2.6 Atomic force microscopy

Atomic force microscopy (AFM) scans were collected across the weld region between fibers of select samples [Figure 2(b)], to observe polymer structure and crystallinity at the interface between fibers. To prepare samples for AFM, sections were cut from dog bones using a diamond saw [Figure 2(a)], and then a surface for AFM analysis that included the weld interface [Figure 2(b)] between two fibers was wet-sectioned at room temperature using a UC7 Ultramicrotome (Leica, Germany) to produce a smooth surface, with a roughness of R_a = 0.83 nm as measured by AFM in the amorphous regions of the samples. The cutting direction during sectioning was perpendicular to the weld interface to preserve the weld structure.

AFM images were acquired in tapping mode using a Cypher ES (Asylum Research, USA) AFM (Asylum Cypher Atomic Force Microscope) across the weld region of select samples [Figure 2(b)], to observe the change in morphology of crystalline domains, if any, at the weld interface. Measurements were acquired at room temperature with a silicon cantilever (AC160, Olympus) with a nominal tip radius of 7 nm that was driven on resonance using BlueDrive(TM). The resonant frequency, cantilever stiffness and quality factor of the fundamental cantilever mode was 70.8 kHz, 2.9 N/m and 176, respectively. For scanning, the cantilever was excited using the third cantilever eigenmode, which had a resonant frequency, cantilever stiffness and quality factor of 1.1 MHz, 293 N/m and 683.44, respectively. The third eigenmode is used as the high effective stiffness, and quality factor enables stable and fast scanning over the rough crystalline domains while maintaining low forces owing to the small oscillation amplitudes used, with a typical free air amplitude of 14 nm and setpoint of 10 nm.

Figure 2 Schematic of diamond saw cut location on dogbone (a) and cross section from dogbone cut including weld region imaged with AFM (b)

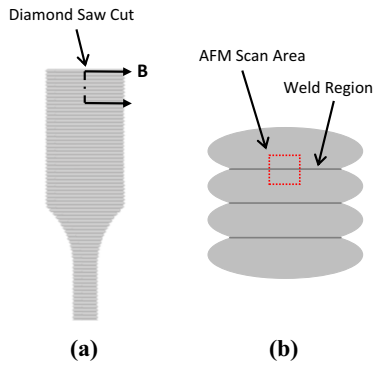

3. Results

The following sections include the results for the two experiments. The first experiment investigates a scan of printing parameters and annealing times and temperatures above T_{cc}. Print quality and crystallinity of these samples are determined using MicroCT and DSC, respectively. Tensile testing determines how print quality and crystallinity impact mechanical properties of the samples. The second experiment investigates annealing above and below T_{cc} at multiple points over 12 h. Porosity and crystallinity are quantified using MicroCT and DSC, respectively. Tensile testing determines how the porosity and crystallinity impact mechanical properties. Finally, AFM is used on select samples to observe polymer morphology and crystallinity in the weld region.

3.1 Scan of printing parameters and annealing

The following section presents the results for the first experiment investigating a scan of printing parameters and annealing times and temperatures above T_{cc}.

3.1.1 Microcomputed tomography print quality

MicroCT scans show the print quality (porosity and "macroscopic" connectivity of fibers in dogbones) for all printing conditions (Figure 3). These qualitative images show how the pores in 0.1 mm layer height dogbones are smaller and more numerous while there are fewer, but larger pores in 0.3 mm layer height dogbones. Connected adjacent pores are the same color while disconnected adjacent pores are different colors. Dogbones printed with the faster speed have larger pores that are more likely to be connected, meaning there is a poorer connection between the printed fibers. Additionally, the print orientation dictates the directionality of the pores. For XY samples, pores are parallel to the loading direction for tensile testing and they are perpendicular to the loading direction for the YZ samples.

3.1.2 Differential scanning calorimetry

DSC of as provided and annealed PLA filament shows how crystallinity increased with temperature and time (Table 2). Filament annealed at 80°C for 15 min had a slightly higher average crystallinity (4.9%) compared to the filament as provided (4.1%). Increasing the time and temperature increased the crystallinity with annealing at 95°C for 60 min achieving a crystallinity of 23.3%.

Figure 3 Avizo images of porosity analysis on dogbone gauge subsection for print parameters (A-D), colors represent connectivity of adjacent pores

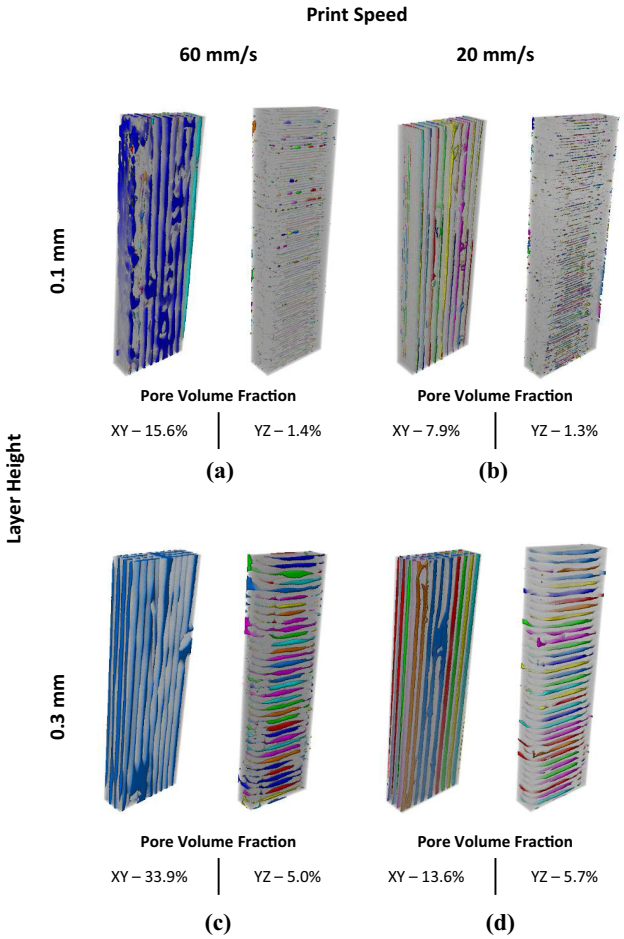

Note: Percent porosity based on airgap volume fraction is listed below each image

3.1.3 Tensile strength

The ultimate tensile strength (UTS) of FFF PLA dogbones was highly dependent on print orientation (Figure 4). The XY samples resulted in a maximum UTS of 53.9 MPa [Figure 4(b) – low layer height, low print speed] and minimum UTS of 41.9 MPa [Figure 4(c) – high layer height, high print speed] while the YZ samples resulted in a maximum UTS of 33.8 MPa [Figure 4(a) – low layer height, high print speed] and minimum UTS of 20.1 MPa [Figure 4(c) – high layer height, high print speed]. There was only a 23% reduction in UTS from XY to YZ samples for A print parameters while in the worst case (D print parameters) there was a 55% reduction.

Annealed dogbones were also tested to see if an increase in crystallinity increased UTS. For the XY samples, annealing resulted in either no change or a decrease ($p < 0.05$) in UTS for all print parameters and annealing conditions (Figure 5). Annealing conditions with higher crystallinity resulted in decreased UTS. For the C – XY printing conditions, the drastic decrease in UTS of the samples annealed at 80°C for 60 min and the samples annealed at 95°C for 60 min falls outside the trend of the other samples. This is likely owing to variability during printing such as build plate levelness or material building up in the nozzle and inadvertently decreasing extrusion. Samples printed with the C print parameters are of poorer quality and more susceptible to a negative impact owing to print variability.

A similar trend was observed in the YZ samples (Figure 6). There was no significant increase in strength with annealing and some annealing conditions resulted in decrease in strength ($p < 0.05$). For the D – YZ printing conditions, the decrease in UTS for the samples annealed at 80°C for 60 min and the samples annealed at 95°C for 60 min falls outside the trend of the other samples. As with the C – XY samples, this is likely owing to variability during printing.

3.2 Annealing above and below cold crystallization

The following section presents the results for the second experiment investigating annealing above and below T_{cc} at multiple points over 12 h. For this section, only dogbones printed with B printing parameters (low layer height, low print speed) were tested given these parameters resulted in the best samples and mechanical properties across YZ and XY samples and with multiple printing efforts.

3.2.1 Porosity

The porosity, as measured and analyzed using MicroCT, of the B print parameter dogbones is plotted against annealing time and temperature for both the XY and YZ samples (Figure 7). There is no clear trend between porosity and the annealing time/temperature. On average, XY dogbones had a higher porosity than YZ dogbones.

3.2.2 Crystallinity

XY- and YZ-oriented dogbones with B print parameters were annealed above T_{cc} (80°C) and below T_{cc} (65°C) for up to 12 h (Figure 8). While samples annealed above T_{cc} increased in crystallinity up to approximately 33% crystallinity for samples annealed for 12 h, samples annealed below crystallization did not significantly increase in crystallinity.

Table 2 Crystallinity of as provided and annealed PLA filament

Annealing temperature (°C)	Annealing time (min)	ΔH (J/g) Average ± STD	Crystallinity (%)
As provided	As provided	1.71 ± 0.55	1.8
80	15	3.83 ± 0.34	4.1
80	60	10.91 ± 1.1	11.7
95	15	20.47 ± 0.65	21.9
95	60	40.87 ± 0.43	43.6

Figure 4 Ultimate tensile strength (UTS) for XY and YZ samples with scanned printing parameters A-D

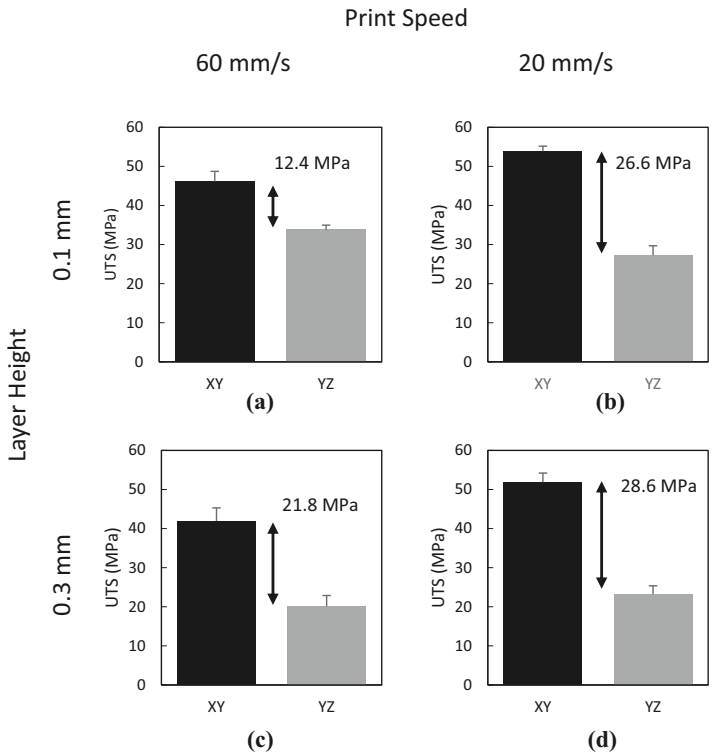

Note: The arrow indicates the difference between mean UTS for samples. Error bars represent one standard deviation, $n = 4$

Figure 5 Ultimate tensile strength for XY samples (A-D print parameters) with scanned annealing parameters

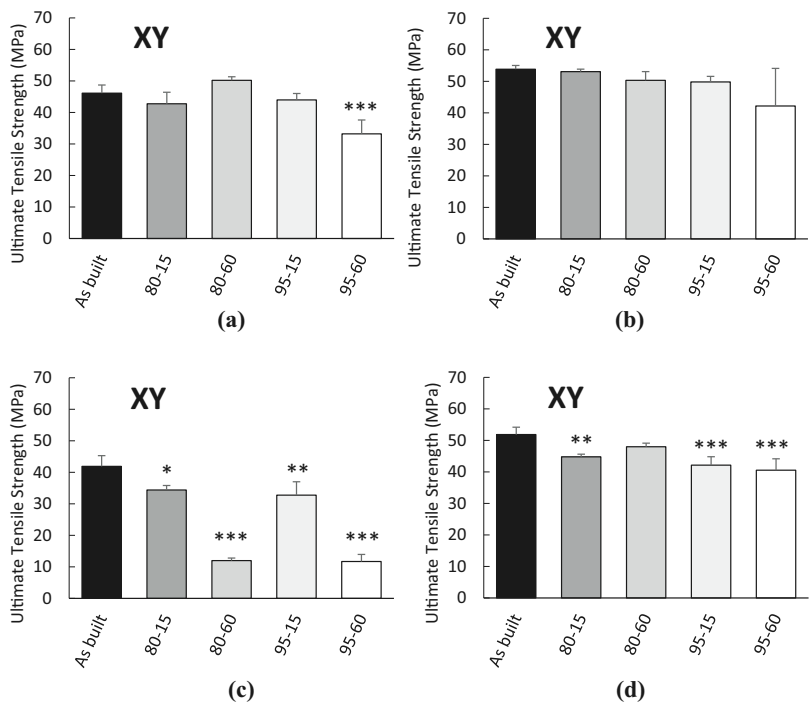

Note: One-way ANOVA with T-test was used to determine significance of annealing compared to the as built treatment, $*p < 0.05$, $**p < 0.01$ $***p < 0.001$. Error bars represent one standard deviation, $n = 4$

Figure 6 Ultimate tensile strength for YZ samples (A-D print parameters) with scanned annealing parameters

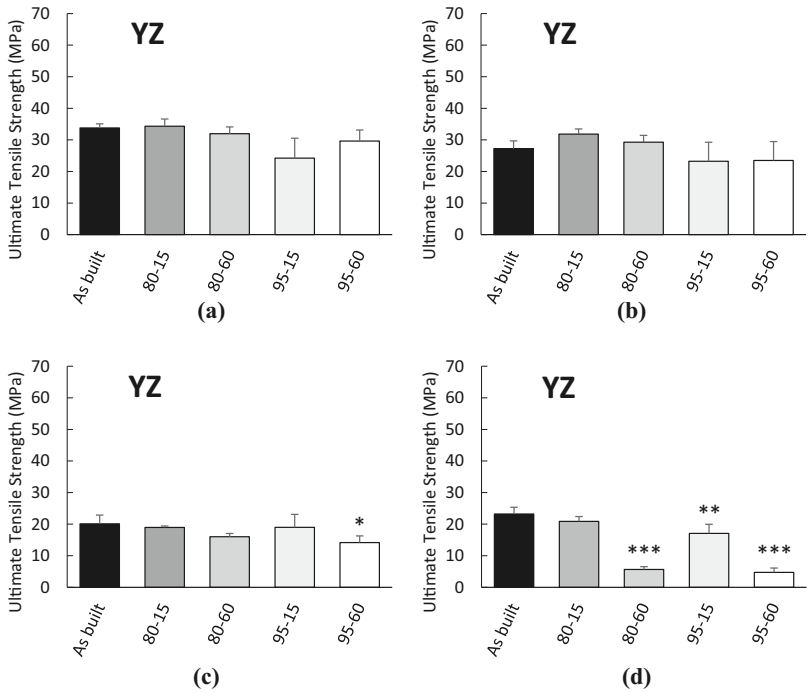

Note: One-way ANOVA with T-test was used to determine significance of annealing compared to the as built treatment, *$p < 0.05$, **$p < 0.01$ ***$p < 0.00$. Error bars represent one standard deviation, $n = 4$

Figure 7 Percent porosity for XY (a) and YZ (b) samples over anneal time

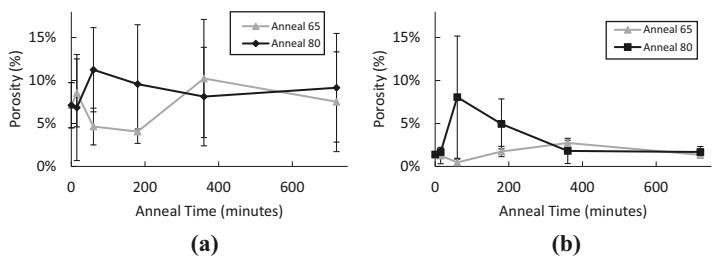

Note: Error bars represent one standard deviation, $n = 3$

Figure 8 Crystallinity percentage for XY and YZ samples as a function of anneal time

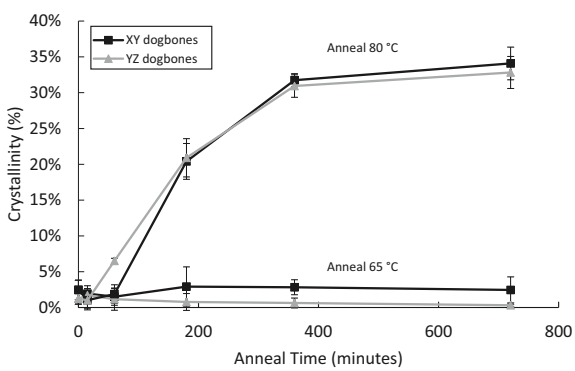

Note: Error bars represent one standard deviation, $n = 3$

3.2.3 Tensile strength

As observed under previous conditions, the UTS of PLA with these annealing conditions was highly dependent on print orientation (all samples tested had B print parameters) (Figure 9). While there was no increase in UTS for samples annealed above T_{cc} at 80°C, there was an increase for samples annealed below T_{cc} at 65°C. A maximum UTS of 64 MPa was achieved for the XY samples and a maximum UTS of 37 MPa was achieved for the YZ samples, both with annealing at 65°C for 6 h.

The UTS data was plotted with crystallinity and porosity to determine the overall relationship between the structure and tensile properties (Figure 10). While crystallinity increased, there is not an increase in UTS. Likewise, samples with improved UTS do not show an increase in crystallinity. There is also no clear relationship between porosity and UTS. The porosity of the YZ samples is lower

Figure 9 Ultimate tensile strength as a function of anneal time

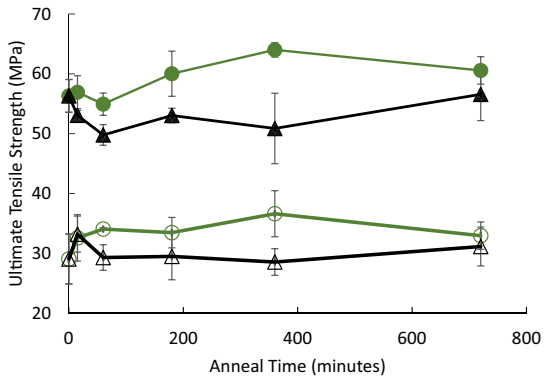

Note: Error bars represent one standard deviation, $n = 4$. Dashed lines represent baseline tensile strength of as printed samples

than the XY samples; however, the UTS of the YZ samples is also lower.

3.3 Atomic force microscopy of as-printed and annealed polylactic acid weld regions

AFM images of select YZ samples demonstrate how the interface at the weld region between filaments exhibits different morphology than the bulk of the fiber filaments as well as the evolution of the PLA with annealing (Figure 11) and a larger scale in Figure 12. (Figure 12) For the as-printed sample [Figure 11(a)], there appears to be distortion at the interface with low crystallinity, possibly owing to incomplete welding during printing. Subsequent annealing of the dogbones reduces the distortion of the interface as the PLA relaxes. For the sample annealed at 65°C for 12 h, the interfacial layer completely "heals," and no discernable interface could be observed in AFM [Figure 11(d)]. For the samples annealed at 80°C, a partially healed interfacial layer can still be observed after 15 min of annealing along with the nucleation and growth of spherulites preferentially on or near the weld interface [Figure 11(b)]. Comparatively, few spherulites are observed in the bulk of the 85°C–15 min sample. For the sample annealed at 80°C for 12 h [Figure 11(c)], spherulites pervade the entire

Figure 11 AFM images of weld regions for as printed (a), 80°C-15 minute anneal (b), 80°C-12 hour anneal (c), and 65°C-12 hour anneal samples with DSC average crystallinity values

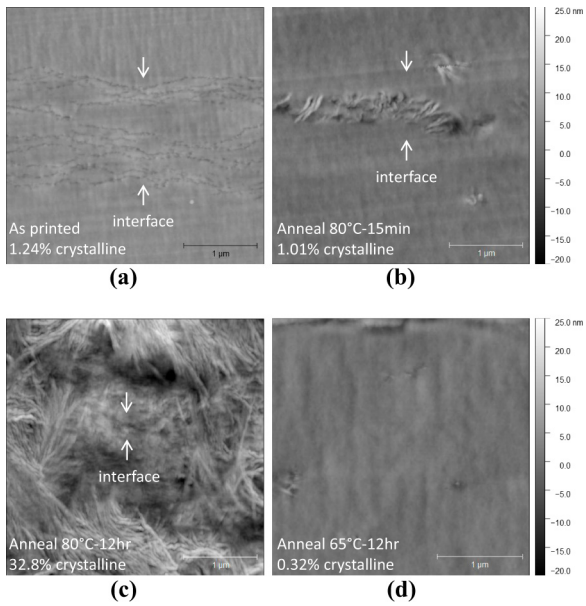

Note: Each scan is 3.5 × 3.5 μm and consists of 512 × 512 pixels collected at a scan rate of 0.5 Hz. The crystalline domains in the sample are observed as feature into the height due to preferential fracture along crystallographic planes during microtoming leading to high surface roughness and distinct structure compared to the amorphous polyme

sample, but the interface in the weld region is still observed as spherulites near the weld interface do not bridge the interface between the welds and a change in local crystalline structure can be observed.

4. Discussion

Previous PLA FFF studies have explored how printing parameters influence tensile properties. Consistent with those studies, we found that the print orientation and the direction of

Figure 10 Ultimate tensile strength as a function of percent crystallinity (a) and porosity (b)

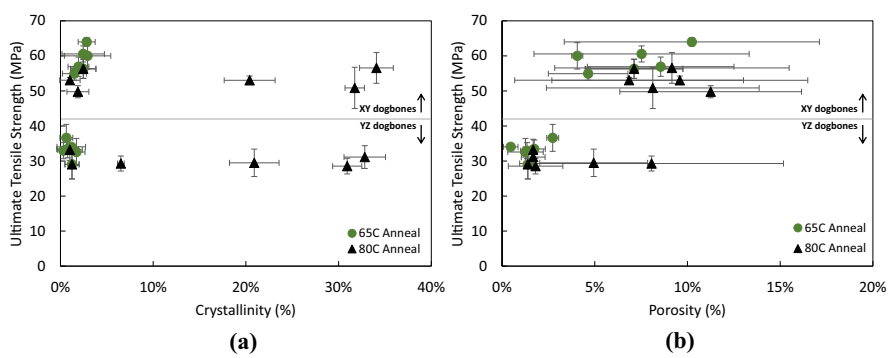

Note: Error bars represent one standard deviation

Figure 12 AFM images of weld regions for as printed (a), 80°C-15 minute anneal (b), 80°C-12 hour anneal (c), and 65°C-12 hour anneal samples with DSC average crystallinity values

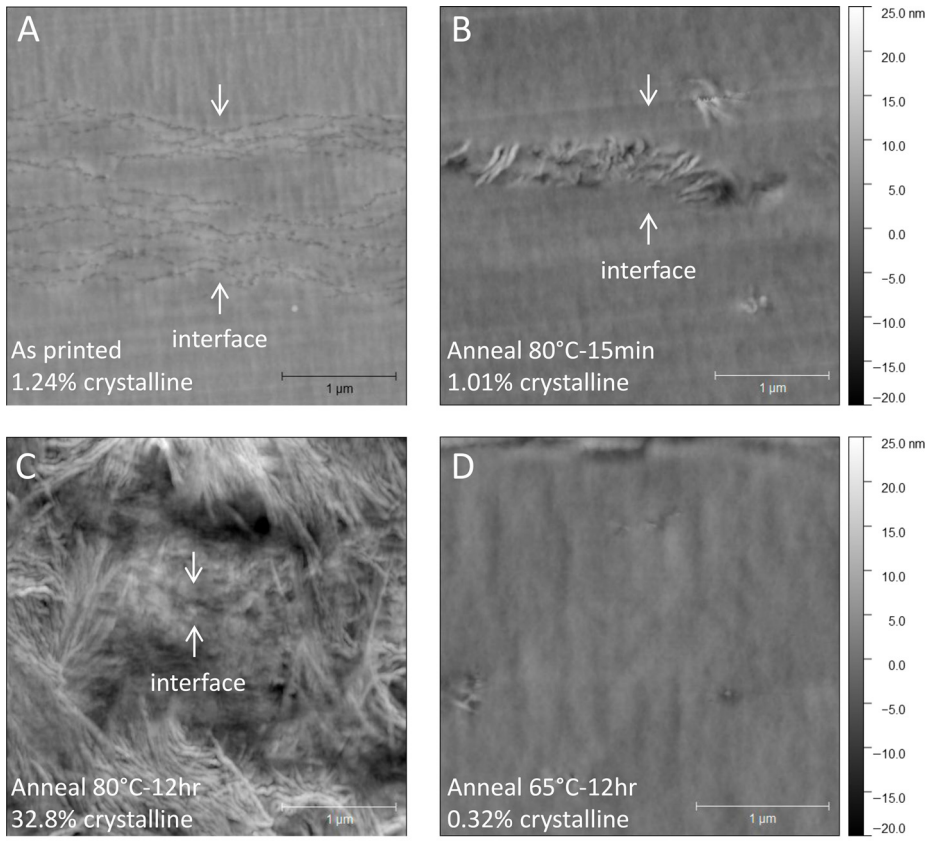

Note: Each scan is 20 x 20 mm and consists of 512 x 512 pixels collected at a scan rate of 0.5 Hz. The crystalline domains in the sample are observed as feature into the height due to preferential fracture along crystallographic planes during microtoming leading to high surface roughness and distinct structure compared to the amorphous polymer

the printed fibers relative to tensile testing direction had the largest impact on tensile strength (Popescu *et al.*, 2018). While print "quality" (measured by porosity) varied based on print parameters (layer height changes the shape and connectivity of the printed fiber and print speed impacts weld development during printing [Coogan and Kazmer, 2017]), the print orientation played a far larger role in tensile strength (Figure 4). These results indicate the inherent interfacial weld strength plays a far greater role than measurable porosity or crystallinity at (but not across) the interface.

Annealing of PLA has been hypothesized as a way to increase the mechanical properties of printed PLA through increasing crystallinity (Mcilroy *et al.*, 2019). However, our data shows that while annealing increases the crystallinity of the sample, tensile strength does not increase and in some cases it decreases as a result of annealing (Figures 5 and 6). This finding suggests that the polymer chains do not co-crystallize across the interface boundaries in the weld, and crystallinity is in fact detrimental to the strength of the dogbone under these print and annealing conditions. Instead, the interfaces between fibers become more brittle and flaw intolerant as crystallinity increases. While it might be expected that samples with fibers oriented in the direction of testing (XY samples) would improve as the welds are parallel to the testing direction, our data still shows there is either a decrease in strength or no improvement. Even though the fibers are oriented in the testing direction, the weak interfaces between those fibers could possibly create flaws that contribute to early failure. Additionally, as the samples crystallize during annealing, there is also a volume change that results in some sample warping that could also contribute negatively to tensile strength.

Our exploration of time-mediated annealing above (80°C) and below (65°C) T_{cc} further investigates the relationship between annealing and improving tensile strength by addressing porosity, crystallinity and weld morphology. While porosity is a factor that impacts the mechanical properties of FFF PLA (Liao *et al.*, 2019), we did not observe a significant change in porosity through annealing at these conditions (Figure 7). The porosity of YZ printed samples was significantly lower than the XY samples but the directionality of the porosity dominated. Porosity in the XY samples was parallel with the printed fibers and the testing direction while porosity in the YZ samples was between fibers and perpendicular to testing direction. In comparing these two

situations, the porosity across the fibers is likely more detrimental when it is in a plane normal to the tensile loading direction. However, with an inherently weak interface, the porosity (even in the plane of tensile loading in the YZ samples) is likely not the largest contributor to material weakness and removing the porosity completely may not result in high strength.

Annealing above T_{cc} increases crystallinity (Figure 8), and influences weld morphology (Figure 11). Previous studies show that chain alignment induced during printing increases the crystallization rate near the interface between filaments during annealing (Mcilroy *et al.*, 2019), leading to spherulites preferentially forming near the weld, as shown in Figure 11(b). This crystallinity limits chain mobility during printing, inhibiting diffusion across the interface and subsequent annealing above T_{cc} then further increases the crystallinity of the samples preventing complete healing of the as-printed weld. While crystallinity could increase the strength of interfaces, the polymer chains need to co-crystallize across the interface, which does not occur in this study. A discontinuous junction promotes brittle fracture. This is also supported by the AFM data where the interface between fibers is still visible even with long annealing times which result in crystallinity pervading the entire sample [Figure 11(c)].

Annealing below T_{cc} heals the weld without increasing crystallinity (Figure 8). The T_{cc} is above the glass transition temperature so polymer chains are mobile but crystallinity does not increase because spherulite growth is inhibited. The limited mobility of the polymer chains in this temperature range between glass transition and T_{cc} enables weld healing without increasing crystallinity. When samples were annealed below T_{cc} but above T_g (at 65°C) there was an increase in UTS with annealing time (Figure 9). The AFM data shows incomplete weld formation at the interface in the as-printed sample but with annealing at 65°C the weld is no longer visible [Figure 11(d)]. This suggests that there could be some "healing" of the interface driven by the annealing relaxing the polymer material and improving cohesion between the fibers.

If annealing that induces crystallinity is used as a post-processing strategy, chain diffusion across the fiber interfaces must be facilitated so that the as-printed weld interface [Figure 11(a)] can first completely heal followed by co-crystallization across the interface. As such, initial annealing of PLA below T_{cc} followed by subsequent annealing above T_{cc} to induce crystallization may be the best approach for optimizing the properties of PLA, but further studies are needed to better understand how crystallinity forms during printing and its role in polymer chain diffusion during interface formation. While it is hopeful that annealing will increase strength with appropriate protocols, it is necessary that the fibers are sufficiently welded so that co-crystallization between fibers occurs, otherwise increasing crystallinity through annealing can result in weaker welds and a decrease in strength.

Further studies need to be conducted on the formation of the weld to improve weld strength and reduce anisotropy, including the relationship between crystallization and polymer chain diffusion (coalescence of fibers). This includes research on the material properties of PLA polymers to tune them for FFF processing and controlling the thermal profile during printing. Srinivas *et al.* have already found that PLA molar mass and L-enantiomeric purity in combination with low print speeds can create stronger interfaces by allowing for polymer chain diffusion before crystallization during printing (Srinivas *et al.*, 2018). The polymer chain diffusion and crystallization processes are highly dependent on thermal conditions. Currently, the FFF printing process has a highly complex and variable thermal profile based on printing parameters and the geometry of the part. More work needs to be done to decrease the variability of the thermal profile the part is experiencing to standardize results and give the user better information in selecting parameters for optimal properties. Current slicing software used to interface with the printer and print parts is optimized for aesthetics and time to produce a print, not consistent mechanical properties. While standard slicing methods were used in this study, new research demonstrates non-planar slicing methods that will enhance design control over the orientation of fibers to further address the issue of mechanical anisotropy (Ahlers *et al.*, 2019). Pursuing research in this area will hopefully result in PLA materials with stronger welds and the ability to tune processing parameters for reliable mechanical properties. Both areas are necessary to create functional PLA devices and products using FFF.

5. Conclusion

This study demonstrates that the print orientation and direction of fibers in respect to loading have the largest impact on mechanical properties in FFF materials owing to weaknesses at the weld. Annealing is explored as a potential post-processing method to improve strength at the weld. Annealing above T_{cc} increases crystallinity while having minimal impact on porosity. However, while crystallinity increases tensile strength in injection molded PLA, strength of FFF PLA either decreases or remains constant, suggesting that co-crystallization across the weld does not occur. AFM images support this finding showing weld interfaces between printed fibers are still visible after annealing above T_{cc}. During annealing, spherulites grow into the bulk of the fiber instead of across the weld interface. Importantly, annealing below T_{cc} shows a moderate but significant increase in tensile strength, while not impacting porosity or crystallinity. AFM images show that the as-printed interface between fibers is not fully cohesive but annealing below T_{cc} heals the as-printed interface resulting in an increase in tensile strength. While annealing has some promise for improving strength at the weld, more research is needed on the formation of the weld and improving fiber coalescence to improve the mechanical properties of FFF PLA and decrease anisotropy between printing directions.

References

Ahlers, D., Wasserfall, F., Hendrich, N. and Zhang, J. (2019), "3D printing of nonplanar layers for smooth surface generation", *IEEE International Conference on Automation Science and Engineering*, doi: 10.1109/COASE.2019.8843116.

Aydin, L. and Kucuk, S. (2018), "A method for more accurate FEA results on a medical device developed by 3D technologies", *Polymers for Advanced Technologies*, Vol. 29 No. 8, pp. 2281-2286.

Beniak, J., Križan, P., Matúš, M. and Šajgalík, M. (2018), "Experimental testing of PLA biodegradable thermoplastic in the frame of 3D printing FDM technology", *MATEC Web of Conferences*, Vol. 157, doi: 10.1051/matecconf/201815706001.

Carrasco, F., Pagès, P., Gámez-Pérez, J., Santana, O.O. and Maspoch, M.L. (2010), "Processing of poly(lactic acid): characterization of chemical structure, thermal stability and mechanical properties", *Polymer Degradation and Stability*, Vol. 95 No. 2, pp. 116-125.

Chacón, J.M., Caminero, M.A., García-Plaza, E. and Núñez, P.J. (2017), "Additive manufacturing of PLA structures using fused deposition modelling: effect of process parameters on mechanical properties and their optimal selection", *Materials & Design*, Vol. 124, pp. 143-157.

Coogan, T.J. and Kazmer, D.O. (2017), "Healing simulation for bond strength prediction of FDM", *Rapid Prototyping Journal*, Vol. 23 No. 3, pp. 551-561.

D'Amico, A.A., Debaie, A. and Peterson, A.M. (2017), "Effect of layer thickness on irreversible thermal expansion and interlayer strength in fused deposition modeling", *Rapid Prototyping Journal*, Vol. 23 No. 5, pp. 943-953.

Fischer, E.W., Sterzel, H.J. and Wegner, G. (1973), "Investigation of the structure of solution grown crystals of lactide copolymers by means of chemical reactions", *Kolloid-Zeitschrift Und Zeitschrift Für Polymere*, Vol. 251 No. 11, pp. 980-990.

Forster, A.M. (2015), "Materials testing standards for additive manufacturing of polymer materials: state of the art and standards applicability", *Additive Manufacturing Materials: Standards, Testing and Applicability*, pp. 67-123.

Li, H., Wang, T., Li, Q., Yu, Z. and Wang, N. (2018), "A quantitative investigation of distortion of polylactic acid/PLA) part in FDM from the point of interface residual stress", *The International Journal of Advanced Manufacturing Technology*, Vol. 94 Nos 1/4, pp. 381-395.

Liao, Y., Liu, C., Coppola, B., Barra, G., Di Maio, L., Incarnato, L. and Lafdi, K. (2019), "Effect of porosity and crystallinity on 3D printed PLA properties", *Polymers*, Vol. 11 No. 9, doi: 10.3390/polym11091487.

Luzanin, O., Guduric, V., Ristic, I. and Muhic, S. (2017), "Investigating impact of five build parameters on the maximum flexural force in FDM specimens – a definitive screening design approach", *Rapid Prototyping Journal*, Vol. 23 No. 6, pp. 1088-1098.

Mcilroy, C., Seppala, J.E. and Kotula, A.P. (2019), "Combining modeling and measurements to predict crystal morphology in material extrusion", *Polymer-Based Additive Manufacturing: Recent Developments, Part 6 – Combining Modeling and Measurements To Predict Crystal Morphology in Material Extrusion*, doi: 10.1021/bk-2019-1315.ch006.

Northcutt, L.A., Orski, S.V., Migler, K.B. and Kotula, A.P. (2018), "Effect of processing conditions on crystallization kinetics during materials extrusion additive manufacturing", *Polymer*, Vol. 154, pp. 182-187.

Peker, A., Aydin, L., Kucuk, S., Ozkoc, G., Cetinarslan, B., Canturk, Z. and Selek, A. (2020), "Additive manufacturing and biomechanical validation of a patient-specific diabetic insole", *Polymers for Advanced Technologies*, Vol. 31 No. 5, pp. 988-996.

Popescu, D., Zapciu, A., Amza, C., Baciu, F. and Marinescu, R. (2018), "FDM process parameters influence over the mechanical properties of polymer specimens: a review", *Polymer Testing*, Vol. 69, pp. 157-166.

Rajpurohit, S.R. and Dave, H.K. (2018), "Effect of process parameters on tensile strength of FDM printed PLA part", *Rapid Prototyping Journal*, Vol. 24 No. 8, pp. 1317-1324.

Rajpurohit, S.R. and Dave, H.K. (2019), "Analysis of tensile strength of a fused filament fabricated PLA part using an open-source 3D printer", *The International Journal of Advanced Manufacturing Technology*, Vol. 101 Nos 5/8, pp. 1525-1536.

Seppala, J.E., Hoon Han, S., Hillgartner, K.E., Davis, C.S. and Migler, K.B. (2017), "Weld formation during material extrusion additive manufacturing", *Soft Matter*, Vol. 13 No. 38, pp. 6761-6769.

Song, Y., Li, Y., Song, W., Yee, K., Lee, K.-Y. and Tagarielli, V.L. (2017), "Measurements of the mechanical response of unidirectional 3D-printed PLA", *Materials & Design*, Vol. 123, pp. 154-164.

Srinivas, V., van Hooy-Corstjens, C.S.J. and Harings, J.A.W. (2018), "Correlating molecular and crystallization dynamics to macroscopic fusion and thermodynamic stability in fused deposition modeling; a model study on polylactides", *Polymer*, Vol. 142, pp. 348-355.

Torres, J., Cotelo, J., Karl, J. and Gordon, A.P. (2015), "Mechanical property optimization of FDM PLA in shear with multiple objectives", *JOM*, Vol. 67 No. 5, pp. 1183-1193.

Tronvoll, S.A., Welo, T. and Elverum, C.W. (2018), "The effects of voids on structural properties of fused deposition modelled parts: a probabilistic approach", *The International Journal of Advanced Manufacturing Technology*, Vol. 97 Nos 9/12, pp. 3607-3618.

Wang, L., Gramlich, W.M. and Gardner, D.J. (2017), "Improving the impact strength of poly(lactic acid) (PLA) in fused layer modeling (FLM)", *Polymer*, Vol. 114, pp. 242-248.

Xue, Y.-Q., Tervoort, T.A., Rastogi, S. and Lemstra, P.J. (2000), "Welding behavior of semicrystalline polymers. 2. Effect of cocrystallization on autoadhesion", *Macromolecules*, Vol. 33 No. 19, pp. 7084-7087, doi: 10.1021/ma000754y.

Yang, L., Li, S., Li, Y., Yang, M. and Yuan, Q. (2019), "Experimental investigations for optimizing the extrusion parameters on FDM PLA printed parts", *Journal of Materials Engineering and Performance*, Vol. 28 No. 1, pp. 169-182.

Corresponding author

Natalia von Windheim can be contacted at: nv19@duke.edu